Introducing Shape Descriptors of Spectral Reflectance Curve (DSRC) for Improving Image Classification Accuracy

[1]Parviz Zeaieanfirouzabadi, [2]Mohsen Salahian

1. Department of Remote Sensing and GIS. Kharazmi University, Tehran Iran. zeaiean@khu.ac.ir
2. Remote Sensing and GIS, Department of Remote Sensing and GIS. Kharazmi University, Tehran, Iran. mohsensalahian@gmail.com

Keywords: Pixel Shape Index, image classification, Accuracy, OLI images.

Abstract

Most algorithms used to extract information about objects in satellite images rely on data derived from groups of pixels (i.e. Training sites). The information space pertaining to individual pixels. However, remains largely underutilized. Here, we introduce a new approach to understanding pixel space by analyzing its shape descriptors derived from the spectral reflectance curve (SDSRC), and we illustrate an application of this concept. Six shape-based feature extraction and representation methods were explored. Among them, the Shape Center of Gravity (COG) or centroid, Area Under Curve (AUC), and the distance between the center of gravity to the Cartesian coordinate center are identified as parameters. We generated images based on these parameters, referred to as Pixel Shape Indices (PSI). PSI images were produced for a section of an OLI Landsat satellite image of the Los Angeles metropolitan area. Twenty-two datasets were created, combining original spectral bands with PSI images, and used for classification via the Maximum Likelihood classification scheme across four land use/land cover types. Classification Accuracy was assessed using the Kappa coefficient of agreement as well as the Hellden and Short coefficients. In most cases, results show improved values for all metrics, indicating enhanced classification performance across all land use / land cover categories due to the integration of PSI features. It is recommended that PSI images be incorporated into various image processing techniques- such as image fusion, filtering, enhancements, and texture analysis- for improved mapping and environmental monitoring.

1. INTRODUCTION

1.1 Background

Feature extraction is a crucial aspect of image understanding, and it has attracted considerable research interests from scientists all over the world. The volume of research appears to have increased in recent years. The methods and algorithms involved in image feature extraction include, but are not limited to, the following (Nixon and Aguado, 2008):
- Low-level feature extraction through edge detectors
- High-level feature extraction by shape matching
- Flexible shape extraction (snakes and other techniques)
- Object description
- Texture description, segmentation, and classification

Satellite image thematic information extraction is a key component of pattern recognition and can be implemented using various classification strategies. Pixel-based and object-based information extraction techniques are the two main categories of these strategies. One of the most challenging topics for remote sensing experts is improving the accuracy of maps produced via image classification techniques. All classification techniques, either using simple algorithms like minimum distance to the mean or sophisticated deep learning models like CNNs, requires suitable input data and information. Scientists have paid significant attention to different types of input data to enhance the accuracy of outputs. Numerous investigators have attempted to improve classification accuracy through the inclusion of various data sources including axillary information and image driven information like vegetation and other spectral indices.
Lu and Weng (2007) reviewed image classification methods and techniques aimed at enhancing classification performance. They concluded that "the effective use of multiple features of remotely sensed data and the selection of a suitable classification method are especially significant for improving classification accuracy, and the spectral response feature is the most important information used for land-cover classification." They summarized approaches for utilizing multiple features of remotely sensed data to enhance classification accuracy, including:
- First, second, and third-order statistics in the spatial domain as texture features, such as Grey-Level Co-occurrence Matrices (GLCM)
- Fractal information
- Geostatistical analysis, including semi-variograms and Gabor filtering
- Fusion of multi-sensor or multi-resolution data, including active and passive remote sensing data
- Various transformation methods, such as fuzzy partitioning, stepwise regression analysis, principal component analysis (PCA), tasselled cap transformation, wavelet transformation, rotational transformation, Gaussian mixture discriminant analysis, normalized difference built-up index, and spectral mixture analysis
- Use of multi-temporal data, including optical and SAR images
- Use of fine spatial resolution data
- Use of hyperspectral data

Additionally, they discussed the usefulness of ancillary data—such as topography, soil, road, and census data—and their integration with remotely sensed data to improve classification performance.
Zhang et al. (2023) introduced a spectral-spatial feature-based index called the Pixel Neighbourhood Similarity (PNS) index to improve classification accuracy. They concluded that "the performance quality of PNS was relatively highest compared to other spectral-spatial features." A variety of information derived from remotely sensed data, such as NDVI, NDSI, NDMI, NDBI, DEM, etc., has been incorporated into satellite images to increase classification accuracy. Pasternak and Pawluszek-

This contribution has been peer-reviewed. The double-blind peer-review was conducted on the basis of the full paper.
https://doi.org/10.5194/isprs-annals-X-5-W2-2025-725-2025 | © Author(s) 2025. CC BY 4.0 License.

Filipiak (2022) evaluated the effect of adding spectral vegetation indices on the accuracy of crop type identification, concluding that most indices significantly improved classification accuracy.

Based on the preceding literature review, no evidence supports the use of a single pixel's spectral profile (curve) to enhance classification accuracy. Therefore, to improve the performance of satellite image classification, this study explores the use of shape descriptors derived from of a spectral curve individual pixels. The employed shape descriptors include the Shape Centre of Gravity (SCG), Area Under the Curve (AUC), and the distance between the centre of gravity and the Cartesian coordinate centre, all of which will be discussed in the following section.

1.2 Conceptual Framework of the Proposed Method

As is evident, previous studies primarily relying on information from neighboring pixels or spectral indices rather than shape descriptors of a single pixel's spectral curve. Milan Sonka et al. (2014) identified four shape representation methods and descriptors for features in an image, including:

a) Region identification
b) Contour-based shape representation
c) Region-based shape representation and descriptor
d) Shape classes

Yang Mingqiang et al. (2008) outlined six approaches for shape-based feature extraction and representation. They provided a detailed explanation of:

1. One-dimensional function for shape representation
2. Polygonal approximation
3. Spatial interrelation features
4. Moments
5. Scale-space methods
6. Shape transform domains

Shape parameters such as the center of gravity, axis of least inertia, digital bending energy, eccentricity, circularity ratio, elliptic variance, rectangularity, convexity, solidity, Euler number, profiles, and hole area ratio are commonly used as filters to eliminate false detections or combined with other shape descriptors to discriminate shapes.

All the above methods use shape information of an image object through different representation techniques (i.e., contour-based or region-based). A comprehensive review of shape representation methods for shape-based object recognition in images was published by Jiang and Zhou (2024).

The spectral reflectance curve of various types of surface materials is assumed to be unique, depending on the similarity of their composition and environmental conditions. Scientists worldwide have attempted to extract valuable information from such curves and their behavior. However, shape descriptors of these curves have not been fully explored or utilized. These descriptors include, but are not limited to, the center of gravity (COG), area under the spectral curve (AUC), X and Y coordinates of the center of gravity of spectral curves, and the distance between the center of gravity and the Cartesian coordinate center. To visually demonstrate these parameters, consider the following spectral reflectance curve prototype:

1.2.1 Area Under Curve (AUC) for the Spectral Profile of a Single Pixel:

The total area under the spectral curve (profile) of a pixel, as shown in Figure 1.

Where the X-axis represents spectral band numbers, and the Y-axis represents reflectance values in percentage.

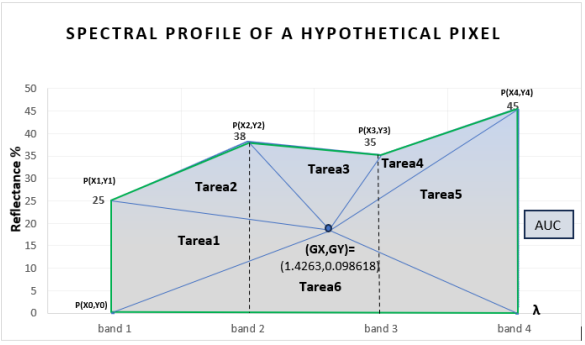

Figure 1. The Spectral curve of a hypothetical pixel of an image. Area under curve (AUC) in gray shade. center of gravity (gx, gy). and six triangles made from this point to all other vertexes (four spectral bands).

The area under the curve can be calculated using Equation 1 (Mingqiang, 2008):

$$A = \frac{1}{2}\left|\sum_{i+1}^{n-1} X_i Y_{i+1} + X_n Y_1 - \sum_{i=1}^{n-1} X_{i+1} Y_i - X_1 Y_n\right| \quad (1)$$

Where A is the are under curve, Xi is the band position in spectrum and Yi is its reflectance value.

1.2.2 Shape Center of Gravity (SCG):

Shapes can be represented either by their region function or by their contour (Mingqiang, 2008), using the position of their center of gravity (Figures 1 and 2):

$$GX = \frac{1}{6A}\sum_{i=0}^{n-1}(X_i + X_{I+1})(X_I Y_{i+1} - X_{i+1} Y_i) \quad (2)$$

$$GY = \frac{1}{6A}\sum_{i=0}^{n-1}(Y_i + Y_{I+1})(X_I Y_{i+1} - X_{i+1} Y_i) \quad (3)$$

Where A is the are under curve, Xi is the band position in spectrum and Yi is its reflectance value.

1.2.2 Areas of Triangles Formed from the Center of Gravity:

In some cases, the area under the spectral curve (AUC) for two or more shapes may be equal, making AUC insufficient for distinguishing between objects. Therefore, it is recommended to use the areas of all triangles formed from the gravity center as an additional shape parameter (Figure 2). The number of triangles formed from the gravity center depends on the number of bands in an image (look at to the number of these triangles in Figures 1 and 2).

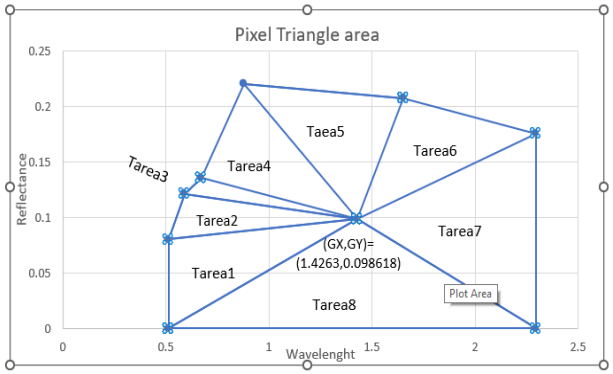

Figure 2. The Spectral curve of a hypothetical pixel of an image. center of gravity (Gx, Gy) and eight triangles made from this point to all other vertexes (five spectral bands).

1.2.3 Distance to the Shape Center of Gravity (DSCG):

In addition to the above parameters, this parameter is also calculated through Euclidean distance between point of central gravity of a shape and center of Cartesian axes (Figure 3).

$$DSCG = \text{sqrt}\,(Gx^2 + Gy^2) \qquad (4)$$

Where DSCG IS the distance to the shape center of gravity, Gx and Gy are x and y coordinates of center of gravity, Xi is the band position in spectrum and Yi is its reflectance value.

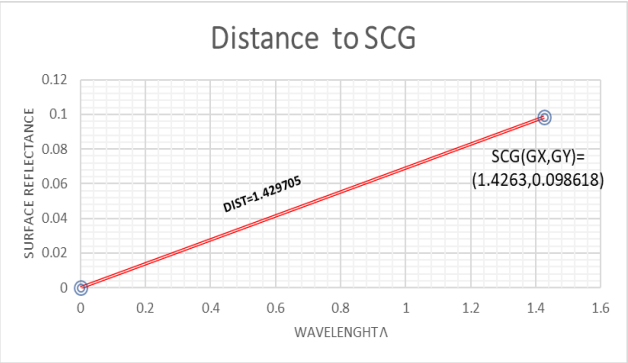

Figure 3. Distance to the Shape Center of Gravity (DSCG) for a given pixel.

2. Martials and Methods

2.1 Study Area

The study area is located south of Los Angeles, California. Surface reflectance Landsat 8 OLI images acquired in 2019 was used as input for further investigation (Figure 4). The data cover 11 spectral bands, ranging from visible to thermal-infrared, with spatial resolutions of 15m, 30m, and 100m. (the USGS Open Access Hub (https://earthexplorer.usgs.gov/). Landsat data are widely used for various applications, including monitoring natural hazards, agriculture, geology, water resources, and climate change. They are highly preferred for remote sensing image classification.

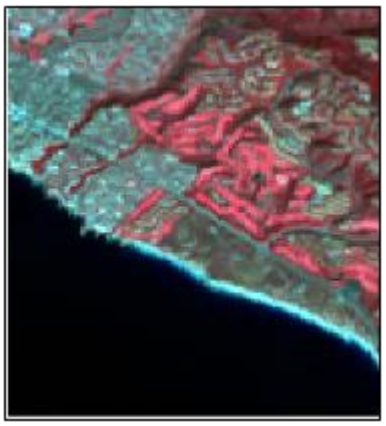

Figure 4. False color composite image of the study area (south of Los Angeles, California).

2.2 Source data

Available land use land cover map prepared by the National Land Cover Database (NLCD) includes different land categories like developed area, forest, water, and wetlands. It covers an approximate area of 4006 km2. It is mainly chosen to evaluate the classification accuracy and testing the proposed method (Figure 5).

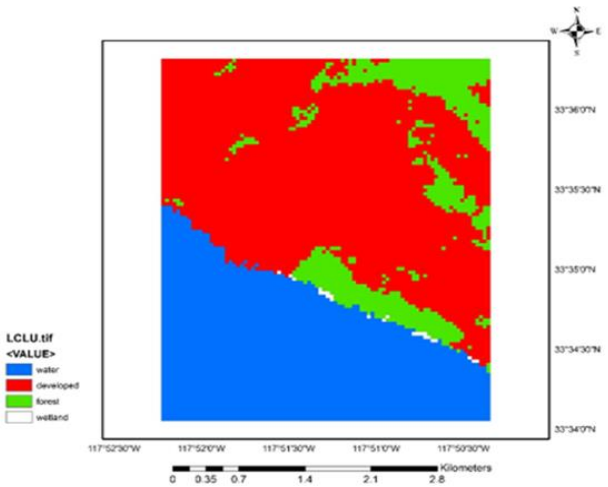

Figure 5. Land use land cover map south of Los Angeles, California (National Land Cover Database | U.S. Geological Survey (usgs.gov).

3. Methodology

3.1 Preparation of Spectral Shape-Based Feature images

Spectral curves for different surface materials have been drawn and feature images of previously discussed parameters (i.e., SCG, AUC, and DSCG) have been produced in a Python environment (Figure 6).

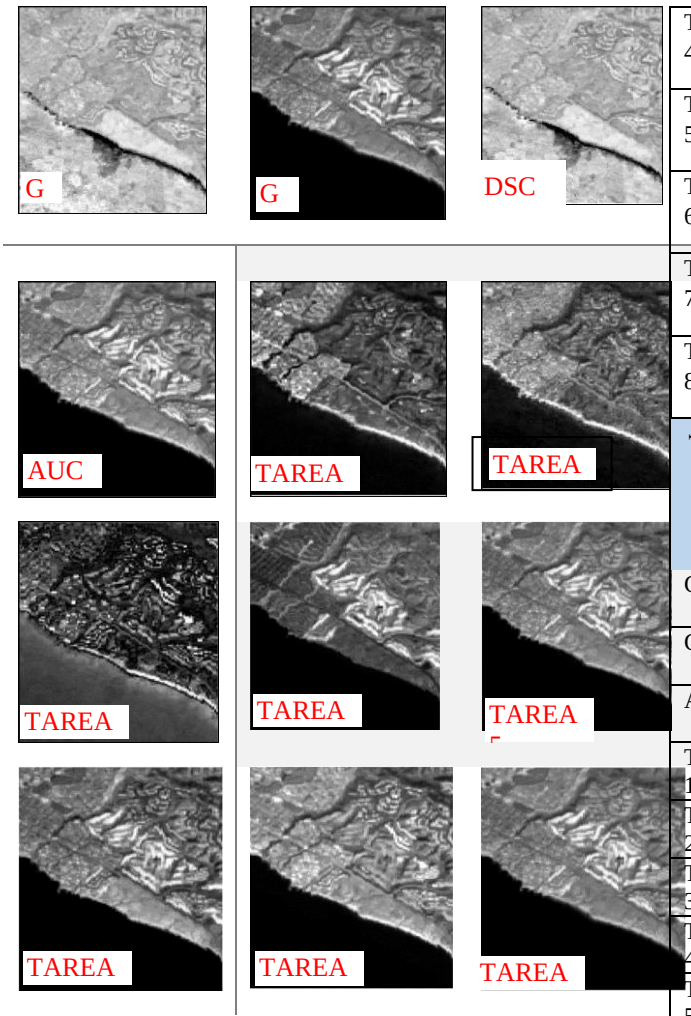

Figure 6. Twelve feature images derived from different parameters (i.e. GX, GY, AUC, DSCG, Tarea1 to Tarea8).

The information derived from parameters of spectral profiles of different land use/land cover are shown in Table 1. As it is clear, different land use/land cover categories have distinct information for all the defined parameters. This allows us to use them for further process.

Table 1. Information derived from defined parameters based on spectral profiles of different land use/land cover

Material/ parameter	rangeland	Barren land	Mountain	Forest	See water	Urban area
Gx	1274	1443	1367	1304	1235	1451
Gy	12.8	17.4	7.30	12.72	2.4	18
AUC	35889	60601	25051	35999	7511	65189
Tarea 1	3429	6987	4276	3169	4341	11740
Tarea 2	232	1766	105	580	1074	1191
Tarea 3	1143	1770	112	1309	414	1214
Tarea 4	9919	5574	3399	10463	84	3021
Tarea 5	5935	7999	3295	5851	631	7980
Tarea 6	2023	7746	2719	3602	180	7523
Tarea 7	4079	13181	4633	3463	1587	16012
Tarea 8	11412	15576	6509	11339	2173	16505

Material/ parameter	Cultivated land	Inland water	Asphalt	Cloud	shadow	Damavand crater
Gx	1301	1190	1407	1275	1361	1350
Gy	14.24	1.963	7.50	25.73	1.95	21.97
Area	41255	5281	26530	85851	6884	77178
Tarea 1	3945	3390	5818	25947	2548	16778
Tarea 2	165	364	233	2167	691	1961
Tarea 3	1243	648	187	2370	85	2397
Tarea 4	11183	204	1929	5729	210	4265
Tarea 5	6599	244	3281	10180	790	9000
Tarea 6	3775	11.6	3097	4562	802	7166
Tarea 7	4468	1103	5764	16301	1398	16032
Tarea 8	12691	1749	6685	22926	1739	19577

To determine whether the information in newly constructed images is similar or dissimilar to that of original images, correlation coefficients were calculated and presented in Table 2.

Table 2. Correlation coefficients of information content of original OLI bands with that of different spectral curve parameters

	B1	**B2**	**B3**	**B4**	**B5**	**B6**
B1	1.00	0.98	0.97	0.61	0.73	0.81
B2	0.98	1.00	0.98	0.72	0.80	0.85
B3	0.97	0.98	1.00	0.70	0.81	0.89
B4	0.61	0.72	0.70	1.00	0.91	0.80
B5	0.73	0.80	0.81	0.91	1.00	0.95
B6	0.81	0.85	0.89	0.80	0.95	1.00
GX	-0.51	-0.52	-0.39	-0.42	-0.41	-0.39
GY	0.70	0.79	0.79	0.97	0.98	0.90
AUC	0.74	0.82	0.82	0.95	0.98	0.93
TA1	0.99	0.96	0.97	0.61	0.76	0.85
TA2	0.90	0.96	0.95	0.71	0.79	0.84
TA3	0.07	0.06	0.11	-0.15	-0.02	0.04
TA4	0.39	0.52	0.49	0.96	0.83	0.66
TA5	0.68	0.77	0.77	0.97	0.98	0.90

https://doi.org/10.5194/isprs-annals-X-5-W2-2025-725-2025

TA6	0.69	0.76	0.77	0.89	0.99	0.92
TA7	0.82	0.87	0.90	0.84	0.96	0.99
TA8	0.70	0.79	0.79	0.97	0.98	0.90
DSCG	-0.50	-0.51	-0.39	-0.41	-0.40	-0.39

A quick look into the Table 2, indicates that the information content of the newly constructed images is not very similar to that of original OLI bands suggesting the potential for improved results with further analysis.

3.2 Classification and accuracy assessment

After generating the images shown in Figure 6, we create 22 datasets comprising original images combined with those derived from the specified parameters. These datasets were then classified using supervised Maximum Likelihood Classification (MLC) with identical training data to ensure the accuracy were comparable across all datasets. Notably, using the same training data not only facilitates fair comparisons but also guarantee that the sole factor affecting classification accuracy is the band information of the input images. To evaluate each classification results, we employed a standard land use/land cover map produced by USGS scientists. Accuracy assessment was carried out using of Kappa coefficient of agreement. In order to compensate for the different interests of users and producers of a classification, certain combinations of producer's and user's accuracy are used. A first such choice is the product and Hellden and Short coefficients (Hellden, 1982, Short, 1980). They give values close to one if both accuracies are high and are close to zero if any of the two is low. (Baatz et al, 2004).

4. Results and Discussion

Classified outputs of the of 21 datasets are presented in figure 7.

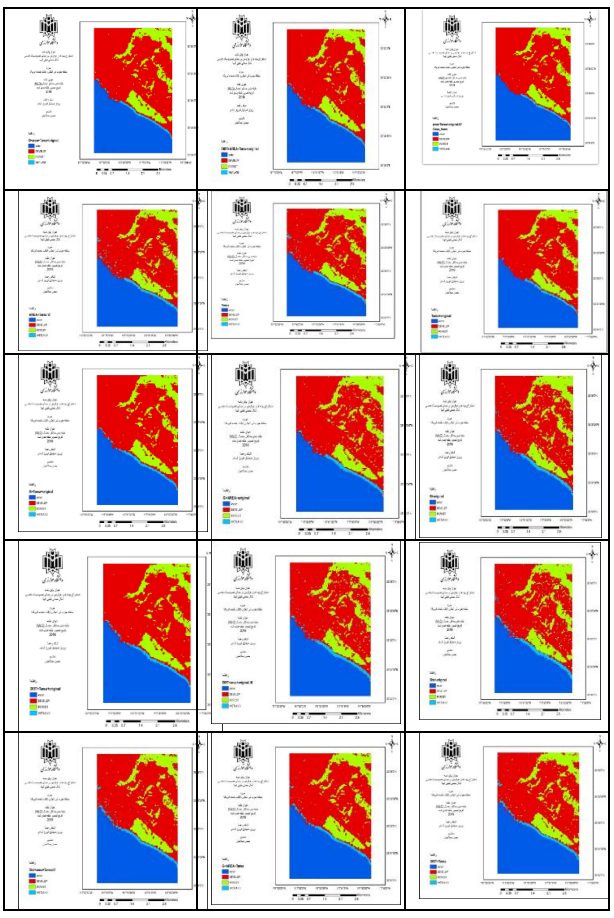

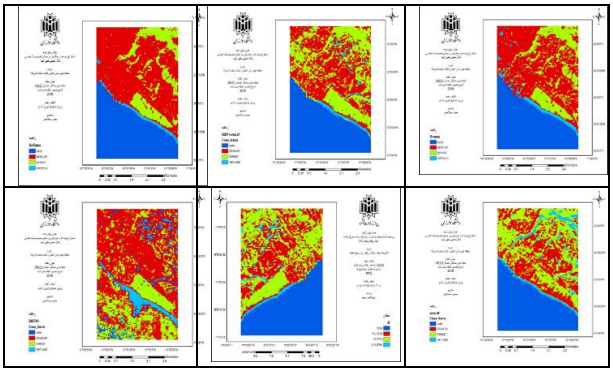

Figure 7. ML classified outputs of 21 different datasets.

The accuracies of classified outputs were assessed using three different methods: Kappa coefficient of agreement, Hellden and Short coefficients applied across different datasets (Table 2 to 4).

Table 2. Kappa coefficient of agreement and User accuracies across different datasets and land use / land cover.

DATASET USED	U-Water	U-developed	U-Forest	U-Wetland	Kappa
Original Bands	1	0.957	0.457	0.2	0.78
AUC, Tarea, Original bands	1	0.953	0.567	0.6	0.85
AUC, Original	1	0.963	0.527	0.27	0.82
Tarea,original	1	0.956	0.565	0.6	**0.85**
Gx,Gy, AUC, Tarea,Original	1	0.945	0.544	0.75	0.84
Gx,Gy, Tarea, Original	1	0.948	0.542	0.6	0.84
Gx,Gy , AUC, Original	1	0.967	0.533	0.37	0.83
Gx, Gy, Original	1	0.966	0.512	0.33	0.82
DIST,AUC,Tarea,Original	1	0.949	0.552	0.6	0.84
DIST,Tarea,Original	1	0.952	0.550	0.37	0.83
DIST,AUC,Original	1	0.966	0.519	0.33	0.83
DIST,Original	1	0.970	0.525	0.3	0.83
DIST,AUC,Tarea	1	0.948	0.521	0.25	0.81
Gx,Gy,,AUC,Tarea	1	0.952	0.528	0.3	0.82
AUC,Tarea	1	0.945	0.545	0.27	0.82
Gx,Gy,,AREA	1	0.960	0.436	0.13	0.75
DIST,AREA	1	0.923	0.256	0.10	0.59
Gx, Gy, Tarea	1	0.955	0.500	0.27	0.80
DIST, Tarea	1	0.951	0.506	0.25	0.80
DIST	0.4	0.710	0.118	0.06	0.17
Gx, Gy	1	0.900	0.210	0.12	0.53
AUC	1	0.891	0.141	0.02	0.46
Tarea	1	0.948	0.521	0.27	0.81

This contribution has been peer-reviewed. The double-blind peer-review was conducted on the basis of the full paper.
https://doi.org/10.5194/isprs-annals-X-5-W2-2025-725-2025 | © Author(s) 2025. CC BY 4.0 License.

Table 3. HELLDEN User accuracies across different datasets and land use / land cover.

DATASET USED	U-Water	U-developed	U-Forest	U-Wetland
ORIGINAL	0.98	0.88	0.58	0.33
AUC,Tarea,ORIGINAL	0.99	0.92	0.66	0.75
AUC,Original	0.99	0.91	0.64	0.43
Tarea,original	0.99	0.92	0.67	0.75
Gx, Gy, AUC,Tarea,Original	0.99	0.91	0.64	0.86
Gx, Gy ,Tarea,original	0.99	0.91	0.64	0.75
Gx, Gy ,AUC,Original	0.99	0.91	0.65	0.55
Gx, Gy ,original	0.99	0.9	0.63	0.5
DIST,AUC,Tarea,original	0.99	0.92	0.64	0.75
DIST,Tarea,original	0.99	0.91	0.65	0.55
DIST,AREA,Original	0.99	0.91	0.64	0.5
DIST,ORIGINAL	0.99	0.9	0.65	0.46
DIST,AUC,Tarea	0.98	0.91	0.62	0.4
Gx, Gy ,AUC,Tarea	0.98	0.91	0.63	0.46
AUC,Tarea	0.98	0.91	0.63	0.43
Gx, Gy ,AUC	0.98	0.86	0.56	0.24
DIST,AUC	0.98	0.71	0.39	0.18
Gx, Gy ,Tarea	0.98	0.9	0.61	0.43
DIST,Tarea	0.98	0.9	0.61	0.4
DIST	0.14	0.73	0.18	0.12
Gx, Gy	0.98	0.64	0.33	0.22
AUC	0.98	0.6	0.22	0.05
Tarea	0.98	0.9	0.62	0.43

Table 4. Short User accuracies across different datasets and land use / land cover.

DATASET USED	U-Water	U-developed	U-Forest	U-Wetland
ORIGINAL	0.96	0.79	0.41	0.03
AUC,Tarea,ORIGINAL	0.98	0.85	0.49	0.23
AUC,Original	0.98	0.83	0.47	0.06
Tarea,original	0.98	0.85	0.5	0.23
Gx, Gy, AUC,Tarea,original	0.98	0.84	0.47	0.32
Gx, Gy, Tarea,original	0.98	0.84	0.48	0.23
Gx, Gy, AUC,Original	0.99	0.84	0.48	0.1
Gx, Gy,,original	0.99	0.82	0.47	0.08
DIST,AREA,Tarea,original	0.98	0.85	0.47	0.23
DIST,Tarea,original	0.97	0.84	0.48	0.1
DIST, AUC,Original	0.99	0.83	0.47	0.08
DIST,ORIGINAL	0.99	0.83	0.48	0.07
DIST, AUC,Tarea	0.96	0.83	0.44	0.05
Gx, Gy, AUC,Tarea	0.96	0.84	0.46	0.07
AUC,Tarea	0.96	0.84	0.46	0.06
Gx, Gy, AUC	0.95	0.76	0.39	0.02
DIST,AREA	0.96	0.55	0.24	0.01
Gx, Gy, Tarea	0.96	0.82	0.44	0.06
DIST,Tarea	0.96	0.82	0.44	0.05
DIST	0.08	0.57	0.1	0
Gx, Gy,	0.96	0.47	0.2	0.01
AUC	0.95	0.42	0.12	0
Tarea	0.96	0.83	0.45	0.06

As evident in Tables 2, in all datasets where the generated supplementary information has been appended to the original image dataset, the classifier's accuracy increased- ranging from **5.95 % to 9.39 %** across the various presented datasets.

An interesting highlight pertains to the datasets containing **Triangle Area**. Not only did the use of this data alone result in a **4.44%** increased in classification accuracy compared to original image dataset, but its derivatives-combined with other geometric information such as **Center of Gravity** of the

spectral curve, etc., - also yield higher classification accuracy than the original image dataset.

It is worth noting that the highest increase in classification accuracy among all datasets was observed in the dataset where **triangle data** was appended to original image dataset.

We now turn to analyzing the variation in classification accuracy for each class across all generated datasets compared to original image dataset. For this analysis, we use two indices: HELLDEN and Short.
As shown in Table 3, all classes across all datasets-where various geometric attributes of the spectral curve were appended to the original image dataset- exhibited an increase in classification accuracy according to **HELLDEN index**.

For the **Water class**, the dataset GX+ GY + Original + AREA and GX+ GY + Original demonstrated the highest classification accuracy improvement, with an increase of **1.49 %**.

For **Urban class**, the dataset AREA + Tarea + Original had the greatest impact, showing a **4.38 %** increase in accuracy.

For **the Forest class**, saw the most substantial positive effect in the dataset Tarea + Original, with an increase of **14.91%.**

Finally, the **Wetland class,** which originally had the lowest classification accuracy in the original image dataset, experienced the highest improvement – **157.14 %-** in the dataset GX+ GY + AREA + Tarea + Original. Notably, the datasets GX+ GY + Tarea + Original, AREA + Tarea + Original, Tarea + Original, and DIST+ AREA + Tarea + Original also showed remarkable improvements of approximately **125%.**

As illustrated in Table 4, In all classes, every dataset in which the original image was augmented with various geometric dataset exhibited an increase in **Short coefficient**. Furthermore, all datasets that include **Tarea** datasets-even without the original image dataset- showed and upward trend in the short coefficient, except in the **water class**, where the value remained unchanged. It is worth noting that the **water class** already had the highest classification accuracy of **96%** in the original image dataset.
In the **Urban class**, the greatest accuracy improvement was observed in the dataset AREA + Tarea + Original with an increase of **8.13%.** The dataset Tarea + Original also showed a similar improvement of 7.21%, indicating that triangle area dataset contributes positively to urban classification.
For the **forest class** as with the urban class, the datasets Tarea + Original and AREA + Tarea + Original, showed increases of **16.399%** and **20.779%** respectively in the **short coefficient**, once again highlighting the usefulness of Triangle area dataset.
Lastly, for the **Wetland class**, which originally had the weakest classification accuracy, we observed a dramatic improvement. The dataset GX + GY + AREA + Tarea + Original which incorporates all data in original image, achieved an increase of **274%** in the short coefficient. Additionally, The DATASETS AREA + Tarea + Original, Tarea + Original, GX + GY+Tarea + Original and DIST+ AREA + Tarea + Original also showed significant increases of **200%**.

References

Baatz, M., Benz, U., Dehghani, S., M., Heyen, M., Höltje, A., Hofman, P., Lingenfelder, I., Mimler, M., Sohlbach, M., Weber, M., Willhauck, G. 2004. eCognition Object oriented image analysis. User Guide. Definiens AG. Definiens Imaging GmbH, München, Germany.

Hellden, U. 1980: A test of landsat-2 imagery and digital data for thematic mapping illustrated by an environmental study in northern Kenya, Lund Univ. Nat. Geog. Inst., Lund, Sweden, *Techn. Rep*. 47.

Jiang, Z., Zhou, C. 2024: Comprehensive Study on Shape Representation Methods for Shape-Based Object Recognition. *J Opt* 53, 1890–1896. https://doi.org/10.1007/s12596-023-01356-x.

Lu, D., Weng, Q. 2007: A survey of image classification methods and techniques for improving classification performance. *International Journal of Remote Sensing*, 28(5), 823–870. https://doi.org/10.1080/01431160600746456,

Mingqiang Y., Kidiyo, K., Ronsin, J. 2008: *A Survey of Shape Feature Extraction Techniques*. Yin, P.-Y. (Ed.). *Pattern Recognition Techniques, Technology and Applications*. InTech. doi: 10.5772/90

Nixon, Mark S., Aguado Alberto S., 2000: *Feature Extraction and Image Processing*, Academic Press, Elsevier Ltd.

Pasternak, M., Pawluszek-Filipiak, K. 2022: The Evaluation of Spectral Vegetation Indexes and Redundancy Reduction on the Accuracy of Crop Type Detection. *Appl. Sci.*, 12, 5067. https://doi.org/10.3390/ app12105067.

Short, *N.M. 1982:* The Landsat tutorial workbook – Basics of satellite remote sensing, *NASA ref. pub. Greenbelt.*
Sonka, M., Havac, V., Boyle, R. 2014: *Image Processing, Analysis, and Machine Vision*, Cengage Learning.

Zhang, K., Chen, Y., Wang, W., Wu, Y., Wang, B., Yan Y. 2023: A method for remote sensing image classification by combining Pixel Neighborhood Similarity and optimal feature combination. *Geocarto International.* VOL. 38, NO. 1, 2158948. https://doi.org/10.1080/10106049.2022.2158948